Extracting geologic information directly from high-resolution full-waveform inversion velocity models — A case study from offshore Trinidad

Nick Benfield[1], Vishram Rambaran[1], Joel Dowlath[1], Tom Sinclair[1], Miles Evans[2], Jamie Richardson[2], Andrew Ratcliffe[2], and Andrew Irving[2]

Abstract

The East Coast Marine Area (ECMA) of Trinidad and Tobago contains producing gas fields where the imaging of seismic data is known to be challenging. This difficulty has been attributed to the combination of the Dolphin Main Fault, with more than 1 km of throw and large velocity contrasts of up to 30% in magnitude across it, and shallow gas and gas clouds causing very high attenuation. These factors lead to difficulties producing reliable and consistent velocity models. Previous velocity models — generated using traveltime tomography — contained inaccuracies that led to poor imaging and structural positioning, resulting in uncertainty when planning exploration and development drilling programs. In an attempt to reduce these uncertainties, a full-waveform inversion (FWI) feasibility study was performed over the most problematic area, with an initial velocity model built from a combination of legacy prestack time and depth migration velocity models and additional first-break refraction tomography. The geologic complexity near the main fault and the associated poor seismic data quality meant this model gave a poor fit between the synthetic and observed data (from a cycle-skipping point of view) at the lowest usable frequency. This led to the idea of applying a diving-wave-driven, offset-stripping workflow across each frequency band in the FWI, going from 3.5 Hz to 7.5 Hz. After successful application on the test area, the workflow was applied to ~1400 km^2 of 3D seismic over the ECMA. The final velocity model is structurally consistent and highly resolved, containing detailed shallow geologic features such as mud volcanoes, well-defined faults, and potential gas anomalies that were not visible on the legacy tomographic model. A blind test of well-pressure data correlates strongly with velocity drops in the FWI model, showing that FWI models can potentially provide very good input to regional pore-pressure-prediction studies.

Introduction

Improving the subsurface image in structurally complex areas is one of the most effective ways to reduce exploration and development risks. The complexity of the geology, coupled with shallow gas, high velocity contrasts across faults, significant velocity anisotropy, and pore-pressure regressions, presents challenges to generating high-quality 3D seismic data sets that can adequately address key issues related to field boundaries, compartmentalization, structural uncertainties, and AVO anomalies. The Dolphin field and the surrounding East Coast Marine Area (ECMA) located in the Columbus Basin, offshore east coast Trinidad (Figure 1a), is one such complex area with poor seismic image quality (Figure 1b). The Dolphin gas field was discovered in 1976 and to date has been producing gas continuously from Pleistocene-age reservoirs. The success and productivity of the Dolphin field have kept possibilities open for other exploration opportunities, both in the shallow section and deeper. Quantifying resources and understanding and reducing risk are critical to the success of targeting any new opportunities. Good-quality 3D seismic data is possibly the most cost-effective way of achieving these goals, and it can also be used as a data set to understand and build dynamic and static reservoir models.

This paper focuses on improving the seismic data image by using full-waveform inversion (FWI) to refine the shallow

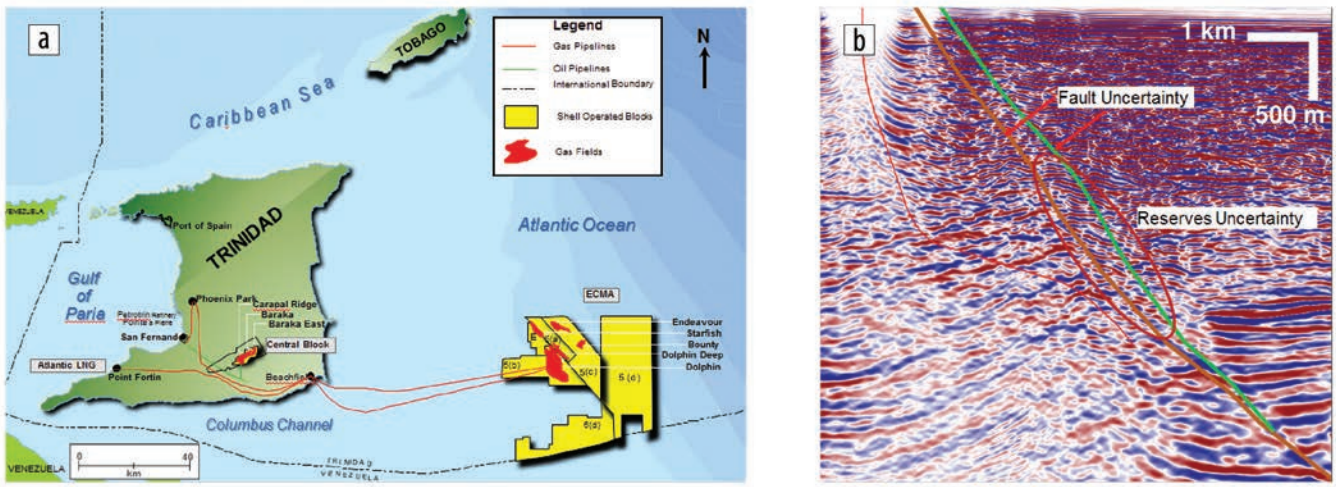

Figure 1. (a) Location map showing the Dolphin field and the ECMA region, offshore Trinidad and Tobago, and (b) typical seismic section from the area showing poor imaging quality and reflector uncertainty.

[1]BG-Group (a wholly owned subsidiary of Royal Dutch Shell PLC).
[2]CGG.

http://dx.doi.org/10.1190/tle36010067.1.

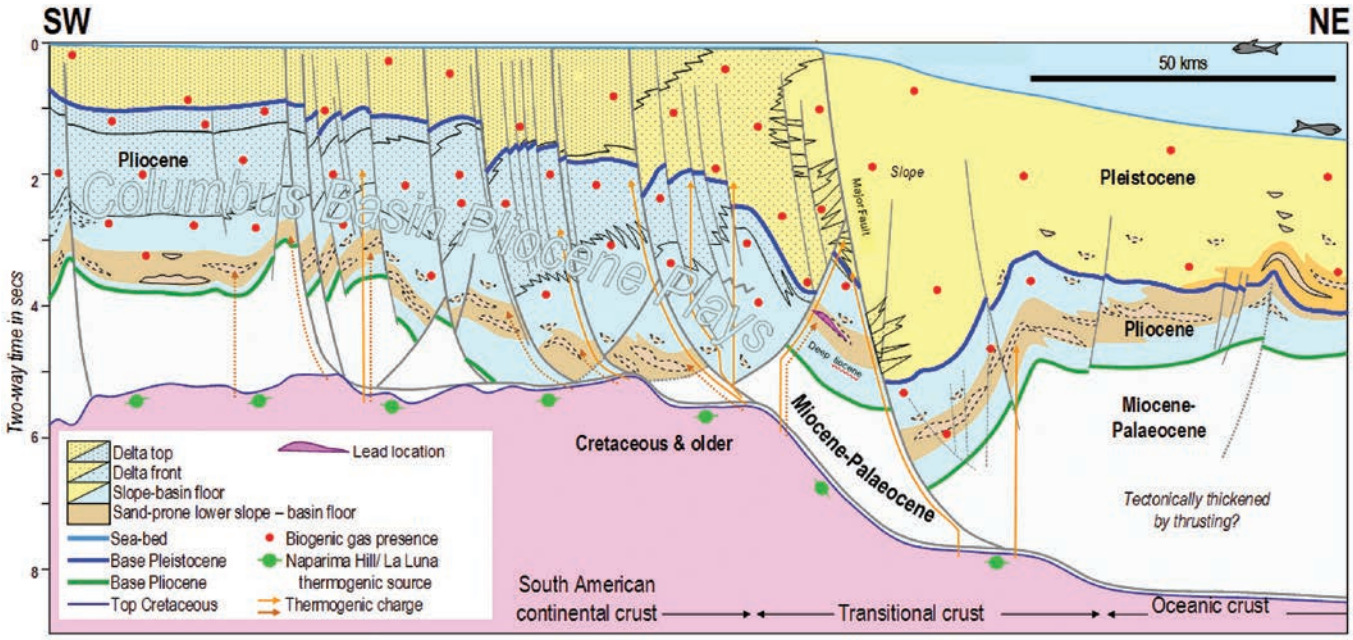

Figure 2. Geoseismic section showing the sedimentary deposition and faulting structure in the region.

velocities and also describes geologic information that can be inferred directly from the resulting velocity model. In this paper's first half, the geology of the region is introduced, then the imaging issues, before describing the FWI methodology and results. The paper's second half discusses interpretational aspects of the FWI velocity model and highlights its use in a blind pore-pressure-prediction (PPP) test of well data.

Geologic overview

The complexity of the Columbus Basin is related to its structural and depositional history. The basin was formed by regional strike-slip interaction between the South American and Caribbean tectonic plates. The dextral motion of these two plates has resulted in transpressional convergence that has generated a deep-seated northeast-southwest fold and fault trend. This trend has been overprinted by an extensive growth-fault array that was superimposed on the system due to sediment loading.

The sedimentary column of the eastern Columbus Basin consists predominantly of thick Pleistocene and Pliocene unconsolidated sands, silts, and clay stones derived from the proto-Orinoco delta and deposited rapidly as part of a shallow-marine, wave-dominated shore face/shelf complex. The Dolphin field consists of a series of stacked Pleistocene sands deposited in a shallow marine environment within a three-way dip closure against the Dolphin Main Fault (Figure 2). This fault forms the eastern boundary of the field and has a northwest-southeast orientation and downthrows to the east with its fault plane dipping between 50 and 60 degrees. It has a throw of up to 8000 ft (2.4 km). The Dolphin Back Fault forms the western boundary and has a throw of up to 4000 ft (1.2 km).

Imaging issues

Previous effort was placed on improving seismic data quality by reprocessing a 1998 legacy 3D seismic data set with new and improved processing algorithms, with such algorithms being designed to improve the signal-to-noise (S/N) ratio and frequency bandwidth of the seismic data. However, acquisition parameters, equipment, and survey designs have evolved over the years to provide better-quality seismic data. In particular, older acquisitions may not be tailored to address the subsurface problems encountered here related to shallow gas, disequilibrium compaction, pore-pressure regressions, mud diapirism, velocity anisotropy, and fault shadows. Therefore, after several rounds of reprocessing the legacy 3D seismic data set — with little improvement in final data quality — a new 3D seismic survey was acquired in 2012 using longer offsets, deep-tow steerable streamers, and larger air guns. As expected, the initial processing of the 2012 data showed significant improvements in imaging quality when compared with the legacy 1998 data. Despite this uplift, this new seismic data still highlighted similar issues inherent in the legacy data, such as poor reflectivity and fault definition, as well as structural uncertainty (Figure 1b). Poor seismic imaging over the Dolphin field has always been attributed to the acquisition parameters, high cable feathering, and the direction (azimuth) of acquisition; the 2012 data show that these might not be the only factors to blame for the poor image quality. In addition, the poor data quality led to uncertainty in the prestack time and depth migration (PSTM and PSDM) velocity models derived from traveltime tomography, especially in the near surface. To improve the near-surface velocity model and, consequently, the overall imaging, an FWI project was undertaken as this emerging technology has the potential to correctly identify shallow velocity complexity associated with the shallow gas and extensive faulting.

Full-waveform inversion

FWI velocity model updates are based on a comparison between observed data (acquired in the field) and synthetic data (modeled using the two-way wave equation), typically via a least-squares cost function. This mismatch is then iteratively minimized through updates to the velocity model (Lailly, 1983; Tarantola, 1984). We use the time-domain, preconditioned, steepest-descent algorithm as described in Warner et al. (2013) and updated by Ratcliffe et al. (2014). FWI of reflected wave data was not considered for the deeper part of the velocity model due to the expected uncertainties in the deeper macromodel, making it potentially

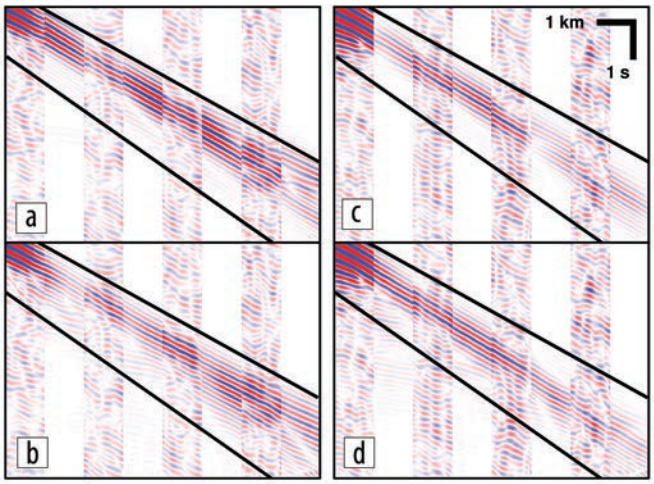

Figure 3. Comparison of two sets of observed field data and modeled shot gathers, both filtered to 4 Hz, where each column is from a different common shot location: (a) and (c) synthetics coming from the starting velocity model, and (b) and (d) synthetics coming from the final FWI velocity model. To aid the cycle-skipping comparison, we plot the data interleaved (real/synthetic/real/synthetic/…) in 1 km offset intervals. The solid black lines indicate the mute used in the inversion, although the data are displayed here unmuted. The data in the left-hand column are from a slightly better-quality area, whereas the right-hand-column data are from a slightly poorer-quality area. In the interests of fair comparison, neither are the extremes of these cases.

unreliable at present. However, a deeper reflection tomography is planned as a separate, post-FWI, processing project.

Due to their short acquisition cable length, shallow shot and receiver depths, and very noisy shot records, the legacy 1998 seismic data are not really appropriate for FWI studies. In an effort to try to use all available data, they were incorporated into the current workflow but with no benefit. Hence, these data were dropped from this analysis, and the FWI update was driven only by the data acquired in 2012. This survey had shot and receiver depths of 10 m and 16 m, respectively, with 10 cables towed, each 100 m apart and 8.1 km in length. The deeper-than-normal shot/receiver tow provides better-quality low-frequency data than from a shallower tow. For example: a simple 1D analysis of the shot and receiver ghost effect at 5 Hz indicates an approximate three times increase in signal strength due to moving the shot from 6 to 10 m, and the cable from 8 to 16 m, due to the reduced ghost notch at low frequencies, irrespective of any reduced recording noise from the deeper tow. The cable length has a direct impact on the penetration depth of the diving waves that drive the FWI, with longer cables acquiring deeper-penetrating diving waves. The shots were acquired in a 25 m flip-flop configuration. Existing infrastructure around the Dolphin platform meant some orthogonal lines were also shot (and used) to provide additional coverage in this area.

Preprocessing of the 2012 data identified swell noise and cable noise caused when the vessel veers away from the platform. This led to the application of a sparse dipole Tau-P process (Ray et al., 2014) to denoise the shot gathers and a simple dip filter to attenuate negative dips on the shot gathers. Rig and seismic interference noise was identified but was observed to mainly be at frequencies higher than the range used by FWI. The only other preprocessing was an inner and outer mute and a bandpass filter to highlight the diving-wave data and frequencies of interest to FWI, respectively.

The source wavelet for FWI was estimated using the inversion method of Davison and Poole (2015), in which a clean direct arrival is isolated on the shot gathers from the deeper-water part of the survey and subsequently inverted to give a ghost-free signature. This resulting wavelet is a more realistic match to the real data, especially at low frequencies where it contains more oscillatory bubble energy than a standard (modeled) far-field signature. Otherwise, there was good agreement with this standard signature.

The diving wave penetration was modeled using a ray-traced analysis through a legacy velocity model at various locations throughout the survey. The maximum depth of penetration, and hence the FWI update, varies significantly depending on the local velocity and geologic environment, from depths of ~1 km on the footwall side of the Dolphin Main Fault to 2.5 km on the hanging-wall side. The penetration depth was also used to generate the FWI penetrating horizon on the hanging and footwall of the Dolphin Main Fault. The average depth of the shallowest producing reservoir interval is ~1.7 km on the footwall and ~3.0 km on the hanging wall. After this initial quality control (QC) of the diving waves, a spatially dense and regular ray-tracing analysis meant we could construct an "FWI penetration" horizon that could be used to taper the FWI updates back to the starting model in subsequent work.

One of the key a priori requirements in FWI is that the observed and modeled data generated from the starting velocity model are not cycle-skipped — i.e., they do not differ from one another by more than a half cycle (see, for example, Virieux and Operto [2009]). Given the combination of poor seismic data quality, uncertainty in the starting velocity model, and expected complexity of the final velocity model, this was always likely to be the greatest problem in this study. Consequently, an initial FWI feasibility project was performed over the area in the survey that was expected to be most complex, namely the region encompassing the Dolphin Main and Back Faults. The legacy PSDM velocity model contained a number of velocity anomalies (bull's-eyes) indicating that conventional reflection tomography could not invert the model in a geologically consistent way. Consequently, the starting velocity model for this feasibility study was built from the combination of legacy PSTM and PSDM velocity models (as the PSTM covered a larger area than the PSDM, including the footwall side of the Dolphin Main Fault) and additional first-break refraction tomography to update the footwall side of the Dolphin Main Fault. Obtaining this starting model was, by itself, an involved process beyond normal FWI requirements. However, even this model only gave acceptable data fits at the lowest usable frequency (from a cycle-skipping point of view) between the synthetic and observed data out to approximately half the maximum offset of 8.2 km (Figures 3a and 3c).

This data fit — or lack of it — led to the idea of devising a diving-wave-driven, offset-stripping workflow across each frequency band in the FWI, starting from 3.5 Hz and going up to 7.5 Hz in 1 Hz increments. The offset stripping involved multiple passes through the data, starting from 4 km maximum offset and going to the maximum cable length in 1 km increments in each frequency band. Clearly, this is a heavy sequence involving multiple passes through the data; to make this exercise even more challenging, all of the shots in the vicinity of the two Dolphin faults could not be used at the very start of the FWI iterations. The

reason for this is that the Dolphin Main Fault was not a sharp interface, so diving waves close to the fault acquired in either a perpendicular or parallel direction were distorted, and therefore shots had to be "drip-fed" into the inversion as the model improved around the faults. The good news was that this sequence, although intensive, did seem to solve some of the velocity complexity in the shallow section well probed by the diving waves. Overall, it gave a geologically plausible velocity model that improved the structural image and generated modeled shots that were an improved match to the observed data. For reasons of space, we do not show these test results here and only show the final production results. Recent developments in the area of cycle skipping, if proven effective, could provide further potential benefit (for example, Luo and Sava, 2011; Ma and Hale, 2013; Warner and Guasch, 2014).

Anisotropy is another key driver for successful FWI. In this area, we approximate the anisotropy regime with a tilted transverse isotropy (TTI) model in which the delta and epsilon volumes (Thomsen, 1986) are smooth and have delta values derived from the available well data, with their maximum values reaching 9% and 13.5%, respectively. The angles in the TTI model come from smooth structural dip fields. Below the reservoir, these dips are flooded back to zero due to the large amount of structural uncertainty on the imaged data at depth. Given the complications due to data quality, the starting model, and an involved workflow, we choose to honor the existing anisotropy model in this work rather than attempt to invert or improve it. An FWI or reflection tomography anisotropy update is anticipated to be one of the topics of future investigation.

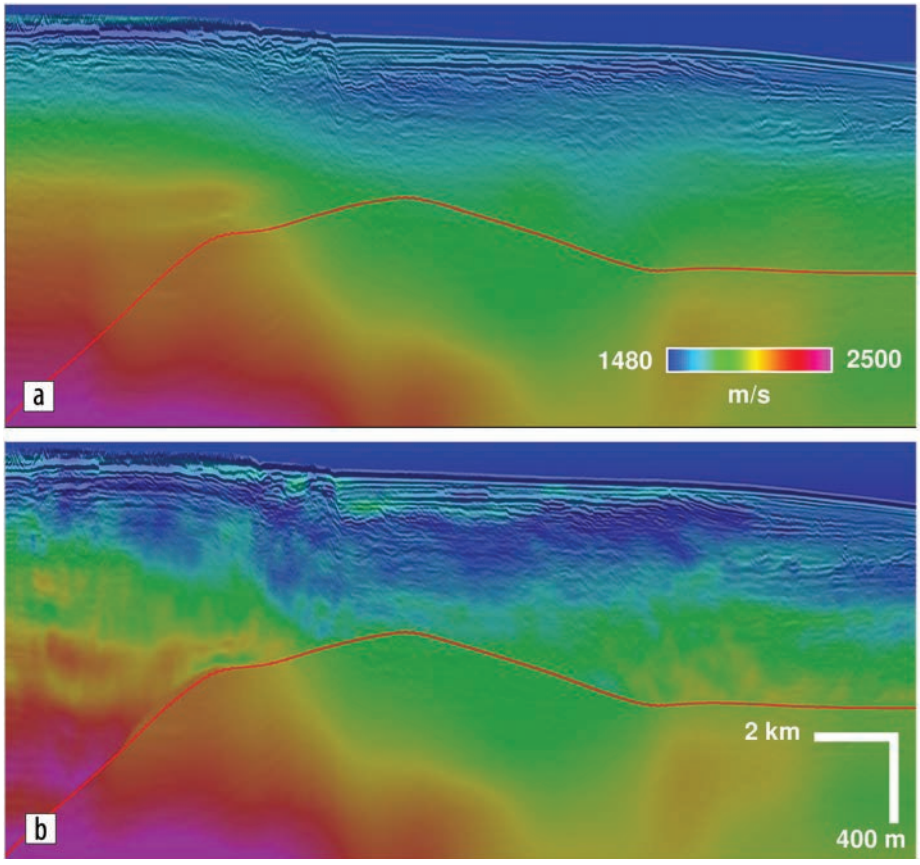

Figure 4. Comparison of velocity models for an inline through the Dolphin area: (a) starting velocity model and (b) FWI velocity model. A migrated stack is overlaid to aid the interpretation, while the red horizon is the limit of the FWI update derived from a dense diving-wave analysis. This display very clearly shows the extent and thickness of the shallow velocity inversion.

After success of the workflow over the Dolphin test area, four more swaths encapsulating the geologic diversity of the region indicated that this bespoke FWI workflow could be run successfully across the entire 2012 acquisition area. Hence, production work using this sequence was run over the full 3D data set of ~1400 km^2 of full-fold data. During this production phase, careful QC was run at each of the frequency milestones to gain confidence in the evolving velocity model. The main QCs were Kirchhoff-migrated images, but modeled shots were also compared to the recorded shots to check that the alignment continued to improve as more offsets and higher frequencies were used. Figure 3 shows an interleaved comparison of the observed data with initial and final modeled shots from a good and poor data-quality region demonstrating an improved match with the real data. The output from FWI showed a mild sail-line-based footprint, which was attenuated by the use of a *k* filtering-based workflow (Jones et al., 2013). This footprint and attenuation technique is typical for streamer geometries and was applied to the whole of the survey and independently for the region around the Dolphin platform that used the orthogonal sail lines. Figure 4 shows the starting velocity model and FWI update for a section through the complex Dolphin Fault area. Clearly, we see a significant increase in the resolution of the FWI model that correlates with the observed geologic features. Figure 5 shows a Kirchhoff imaging comparison as a QC of our results generated from the starting and final FWI velocity models. There is a general shallowing of reflectors, together with some improvement in both the structural form and strength of reflectors in the migrated image. The deeper velocity-model update and subsequent reimaging is beyond the scope of this paper.

Geologic features in the FWI model

The velocity model generated from the FWI project showed many high-resolution features that can be attributed directly to geologic phenomena such as shallow gas, fault definition, and mud volcanoes. This section discusses these interpretational aspects in more detail.

Shallow gas is known to be pervasive in the basin, and traveltime tomography gave hints of the suspected slowdown in velocity (Figure 4a), but, in general, the tomography was not able to resolve any significant velocity contrasts. However, the FWI velocity model showed strong velocity inversions with the velocities reducing back to values close to the water velocity (Figure 4b). Overall,

the gas was more pervasive than originally thought and is seen throughout the FWI model.

The major faults in the area are gravity-driven growth faults with a northeast-southwest strike. These orthogonally intersect west-northwest-oriented to east-southeast-oriented transpressional and transtensional features that are associated with the relative eastward movement of the Caribbean Plate in relation to the South American Plate. The combination of these two structural styles has resulted in the formation of the majority of the hydrocarbon-bearing traps within the Columbus Basin, as well as producing an extremely complex and high-density fault network. The resolution of the FWI velocity model was sufficient to interpret many of the shallow faults directly on the final velocity volume (Figure 6). Figure 6b shows an expanded display of the white rectangle in Figure 6a highlighting clear, high-resolution lineations that, when corendered with the seismic image, show an exact correlation with regions of complex faulting (Figure 6c).

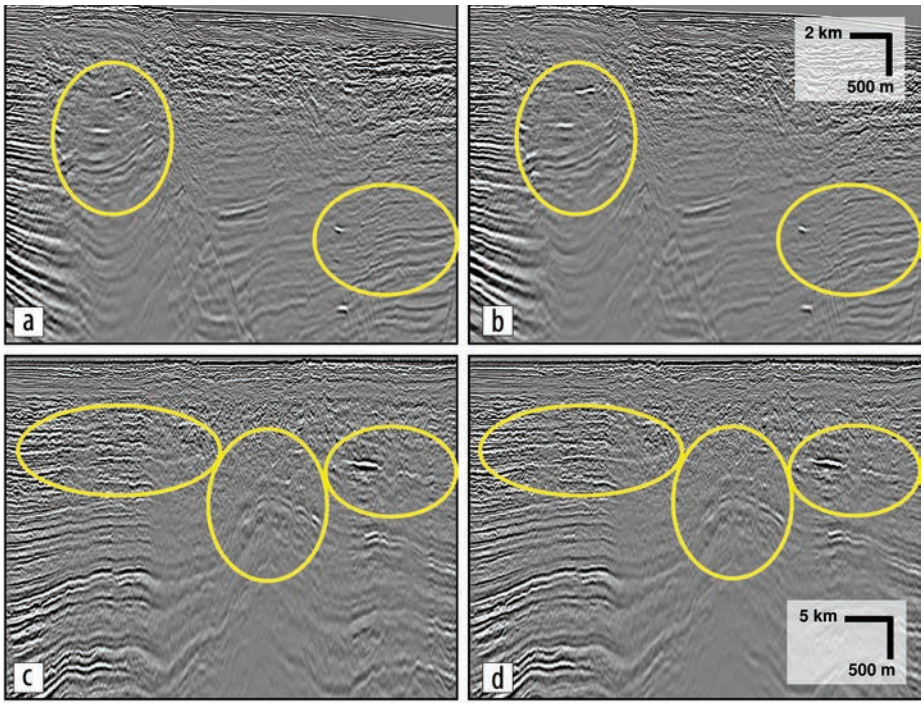

Figure 5. Comparison of Kirchhoff QC migrations that pass through the Dolphin area: (a) inline before FWI, (b) inline after FWI, (c) crossline before FWI, and (d) crossline after FWI. The yellow ovals highlight areas that have stack power or structural improvements after FWI, with reduced velocity distortion in the images.

Throughout the area, there are a series of mud volcanoes/mud diapirism where mobile material has migrated upward until it spreads as a cone on the seafloor before being buried by further sediment deposits. These mud volcanoes are seen throughout the velocity volume as clear velocity contrasts (Figure 7), including the old seafloor itself still visible as the flat reflector at the base of the structure. These contrasts are usually characterized by a velocity speed-up in the feeder neck, associated with the upwelling of denser material than the surrounding sediments. Counter to this, many of the mud volcano/mud diapir's caps are shown as a velocity slowdown, which is attributed to gas that is migrating or has migrated through the mud. An additional benefit of the sharp velocity contrast between the mud volcanoes/mud diapir is that automatic geobody extraction was possible. In this case, we extracted along the 1830 m/s velocity contour and successfully mapped the cone in 3D, including the overhang at the base.

An assessment of shallow hazards, such as the extensive mapping of shallow gas from the very high-resolution velocity model in Figure 4, is important for reducing drilling risk. Given that it is obviously not desirable to drill through thick sequences of shallow gas, this means the velocity model derived from FWI now becomes another key data set in the planning of drilling trajectories.

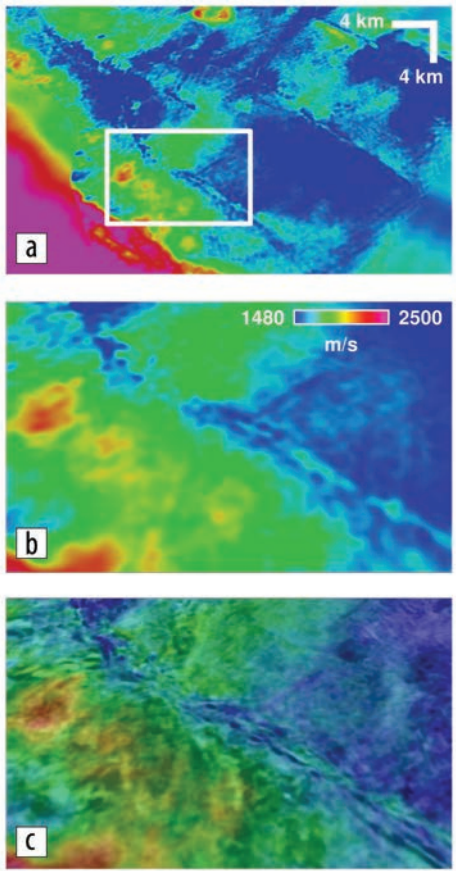

Figure 6. Highlighting the fault complexity in the FWI velocity model: (a) depth slice FWI velocity model, (b) zoom of the region in white on panel (a), and (c) zoom region corendered with seismic image showing the agreement between the velocity and seismic interpretation.

Use of FWI velocities in pore-pressure prediction

A key input to the well-design process is pore pressure, which has an impact on the safe mud weight drilling window and the casing design. Being able to predict the pore-pressure predrill as accurately as possible, while reducing the uncertainty, is a critical part of the well-design workflow. In particular, overpressured

sediments are a common phenomenon in the Columbus Basin, and information about their location and magnitude is very useful to help reduce drilling risk. In this area, the rapid deposition of mudstone-dominated Plio-Pleistocene sediments allows overpressure to be generated by disequilibrium compaction, namely where the sediments cannot dewater quickly enough during burial to allow pressure equilibrium to be obtained. Both the depth of this overpressure onset and the magnitude of the overpressure with depth can vary between wells even when the stratigraphy of the overburden does not change significantly (Figure 8a). The interpretation of these variations is that the overpressure is in a dynamic state, and the pore fluid is being retained in the system by low-permeability mudstones. However, where a well penetrates a clearly defined sand body that is laterally extensive and bounded by a major fault, it allows pressure drainage across that interval. The right-hand side of Figure 8a shows the efficiency of this plumbing system, where a sand at 16,000 ft (~4900 m) true vertical depth subsea (TVDSS) in the Bounty-1 offset well (Bounty field shown on the location map in Figure 1a) is hydrostatically pressured, while the surrounding mudstones are at more than 15 pounds per gallon (ppg) equivalent mud weight (EMW).

The use of velocity data for PPP in mudstone-dominated Tertiary delta systems is a proven technique, in which the velocity response of the mudstone gives an indication of the compaction state of the rock. From this, the vertical effective stress can be estimated using any published PPP algorithm that links velocity to vertical effective stress; for example, Eaton (1975) or Bowers (1995). The steps in a generic PPP workflow for a proposed well would be:

1) interpretation of pore pressure from offset wells using formation pressure tests and drilling data and reports;
2) 1D PPP: use of a wireline or logging while drilling sonic velocity to predict pressure by calibrating the chosen prediction algorithm against the interpreted pore pressure from step 1;
3) 3D PPP: using a fit-for-purpose seismic velocity cube to create a 3D pore-pressure volume and be able to predict the pore pressure away from the offset wells; and
4) integrate the subsurface geologic interpretation.

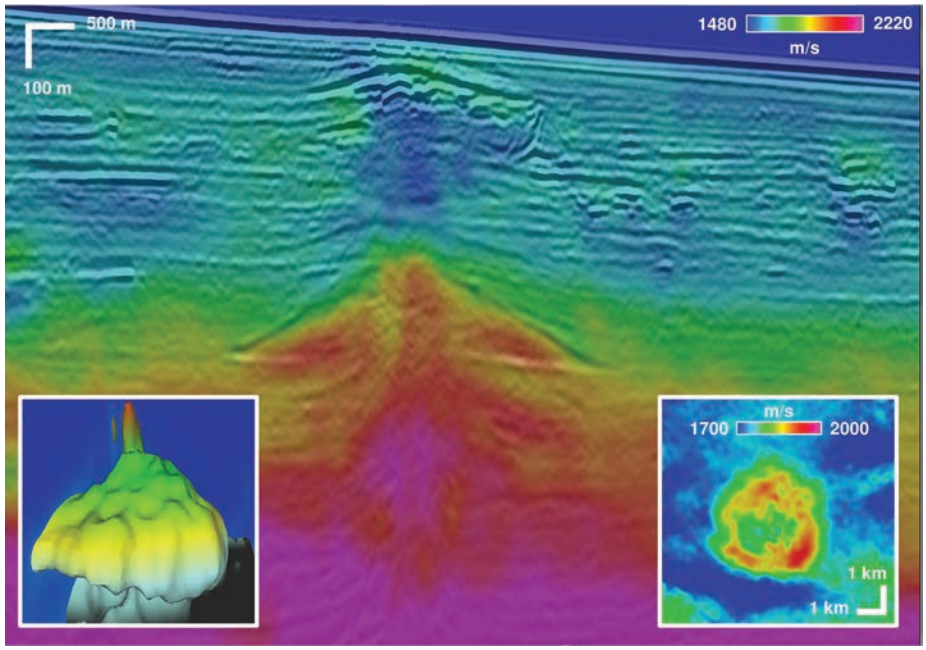

Figure 7. Example of a mud volcano picked out by the FWI velocity model. The lower right-hand inset shows a depth slice through the cone, whereas the lower left-hand inset shows the associated geobody created from the velocity break in the FWI velocity model (something that is not possible from the seismic alone).

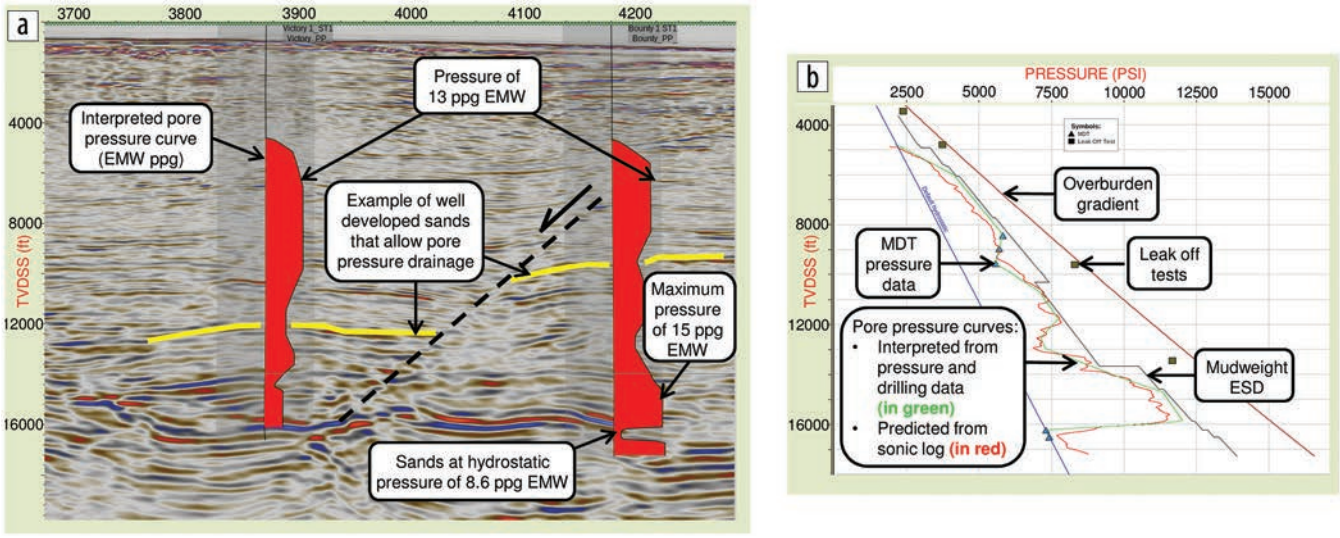

Figure 8. Pore-pressure analysis: (a) two offset wells: Victory-1 (left-hand side) and Bounty-1 (right-hand side), which penetrate a very similar overburden but have different interpreted pore-pressure profiles. (b) The pore-pressure interpretation at the Bounty-1 offset well (green line) and the PPP from the sonic log (red line) demonstrates that good calibration of velocities to pore pressure can be made within this basinal geologic setting.

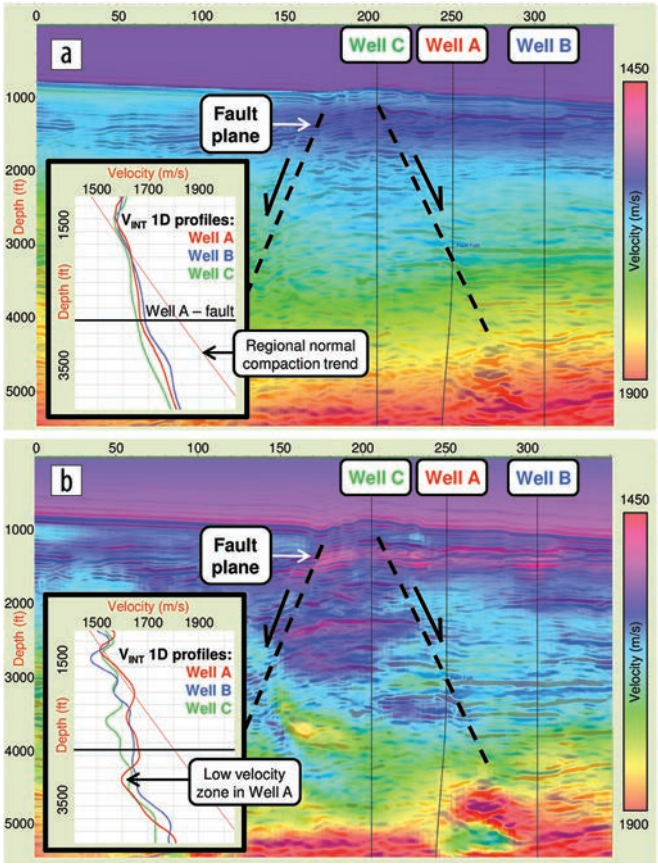

Figure 9. Velocity volumes over the area of interest derived from (a) traveltime tomography and (b) FWI, showing the location of the proposed well path (well A) and two pseudowells in the hanging wall and footwall of the structure.

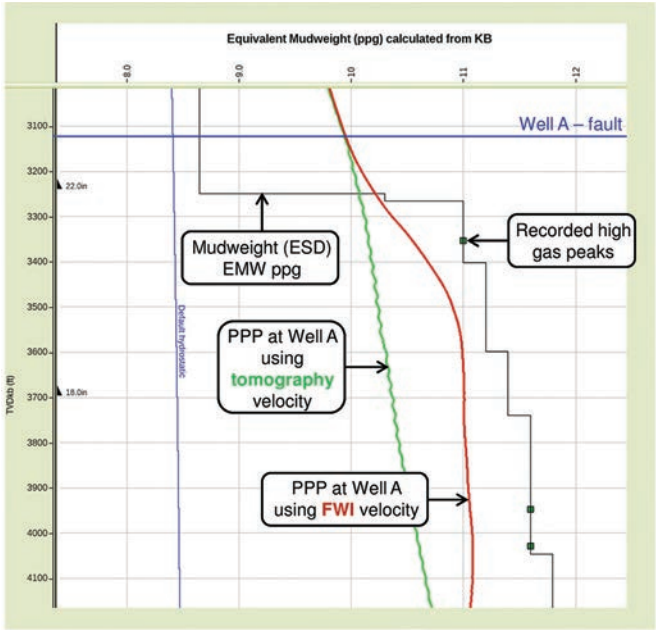

Figure 10. Comparison of PPP results for well location A using the tomography-derived (green line) and FWI-derived (red line) seismic velocity volumes. The gray line shows the actual mud weights used during drilling.

Figure 8b illustrates steps 1 and 2 in this process for the Bounty-1 offset well, showing that a good understanding and calibration of pore pressure exists in this region and, consequently, PPP using velocity data can be used with high confidence.

Turning our attention to step 3 in the workflow above, the velocity inputs are often from the traveltime tomography generated as part of a PSDM project. The resolution of these tomographic methods is such that they only show a smooth velocity profile of the overburden, with subtle changes related to overpressure being absent. However, FWI velocities offer greater resolution, meaning subtle variations in velocities can be observed. Further interpretation then can be made to determine if these changes are geologic and overpressure-related.

Figures 9 and 10 show that the increase in resolution of the FWI velocity volume, compared to the tomography velocity volume, would have helped to (1) reduce the uncertainty of the PPP predrill, and (2) evaluate the risk of the overburden in deciding the well-path trajectory. Specifically, the proposed exploration well (labeled well A on Figure 9) focused on a fault block that had a deep target interval. The preferred well trajectory aimed to drill the hanging wall stratigraphy down to ~3000 ft (~900 m), at which point the well would cross the fault plane into the footwall horst structure. The predrill pore-pressure analysis used offset wells and a tomographic velocity volume that was well calibrated for PPP in the offset wells. A key learning from the offset wells was the dynamic nature of the overpressure in this basin, where it is controlled by the faults, and that a lower pore pressure could occur if clearly defined sand bodies juxtapose against the fault path and act as drainage systems. Equally, the opposite risk could be valid where — if sands are not present — the fault paths could act as pressure seals, and a higher pore-pressure compartment could exist in the footwall compared to the hanging wall. Given that no offset wells penetrated this fault block, the seismic velocities were the primary data in evaluating the pore-pressure risk across the structure.

The traveltime tomography velocities (Figure 9a) show that the footwall (well C) exhibits an overall slower velocity than the hanging wall overburden (well B). However, at the proposed well location (well A) the velocities are closer to the hanging wall profile and, where the well path crosses the fault, there is only 20 m/s difference between the two velocity profiles. The conclusion when using this tomography velocity field was that the pore pressure would not change dramatically on crossing the fault. In comparison, the FWI velocities (Figure 9b) show much more variation across the structure. The absolute magnitude difference between the hanging wall and footwall velocities is greater — on average 100 m/s in the overburden compared to 40 m/s — and there is more vertical variation. At the proposed well location (well A), a low-velocity cell is observed beneath the fault path with the impact of this velocity difference on the PPP seen in Figure 10. The prediction using the FWI velocities shows a greater rate of pressure increase and higher predicted magnitude of pressure (0.7 ppg EMW) compared to that from the tomography velocities. Data gathered during the drilling of the well showed very high gas levels on drilling out of the casing within the footwall, with the mud weight needing to be increased to 11 ppg, and then further to 11.5 ppg, to manage

the formation gas levels. The interpretation was that the formation pore pressure was close to the static mud weight density of 11 ppg between 3300 and 3400 ft (1006–1036 m) true vertical depth kelly bushing (TVDKB).

Even though neither of the velocity models accurately predicted the interpreted pore pressure from the observed drilling data, the higher-resolution velocities from FWI would have allowed the risk of drilling into a higher-pressure footwall compartment to be better assessed predrill. The FWI volume identified a low-velocity cell beneath the fault that translated into a PPP that showed an increasing trend, and a higher predicted magnitude, compared with the pressure prediction from the tomography velocities. No sonic log data was acquired over this key section, and a recommendation for future wells would be to acquire LWD or wireline sonic data where fault paths are crossed to allow even better calibration with the FWI volume and allow for step 2 of the generic PPP workflow to be completed.

Conclusions

We have performed an FWI study on a narrow-azimuth seismic data set acquired in 2012 over the Dolphin field and surrounding East Coast Marine Area in the Columbus Basin, offshore Trinidad and Tobago. This study was challenging due to complex geology and poor seismic data quality, leading to severe uncertainties in the starting velocity model. To overcome these problems, we developed an FWI workflow based on offset and frequency stripping. This workflow's success is measured by the increase in resolution in the updated velocity model; the improvements in the resulting seismic image; the identification and interpretation of a number of shallow geologic features; and a blind FWI-derived velocity prediction of pore pressure that reduces drilling risk by identifying a low-velocity, high-pressure footwall compartment beneath a fault in a target area. This work demonstrates another step in the evolution and maturity of FWI as a technology that can both benefit and derisk exploration and development. TLE

Acknowledgments

We thank BG Trinidad and Tobago (a wholly owned subsidiary of Royal Dutch Shell PLC), CGG, and Chevron Trinidad and Tobago Resources SRL for their permission to publish this work.

Corresponding author: nick.benfield@shell.com

References

Bowers, G. L., 1995, Pore pressure estimation from velocity data: Accounting for overpressure mechanisms besides undercompaction: SPE Drilling & Completion, **10**, no. 02, 89–95, http://dx.doi.org/10.2118/27488-PA.

Davison, C. M., and G. Poole, 2015, Far-field source signature reconstruction using direct arrival data: 77th Conference & Exhibition, EAGE, Extended Abstracts, Th N116 15.

Eaton, B. A., 1975, The equation for geopressure prediction from well logs: SPE 5544.

Jones, C. E., M. Evans, A. Ratcliffe, G. Conroy, R. Jupp, J. I. Selvage, and L. Ramsey, 2013, Full waveform inversion in a complex geological setting — A narrow azimuth towed streamer case study from the Barents Sea: 75th Conference & Exhibition, EAGE, Extended Abstracts, We 11 06, http://dx.doi.org/10.3997/2214-4609.20130830.

Lailly, P., 1983, The seismic inverse problem as a sequence of before stack migrations: Proceedings of the international conference on "Inverse Scattering, theory and applications," SIAM, 206–220.

Luo, S., and P. Sava, 2011, A deconvolution-based objective function for wave-equation inversion: 81st Annual International Meeting, SEG, Expanded Abstracts, 2788–2792, http://dx.doi.org/10.1190/1.3627773.

Ma, Y., and D. Hale, 2013, Wave-equation reflection traveltime inversion with dynamic warping and full-waveform inversion: Geophysics, **78**, no. 6, R223–R233, http://dx.doi.org/10.1190/geo2013-0004.1.

Ratcliffe, A., A. Privitera, G. Conroy, V. Vinje, A. Bertrand, and B. Lyngnes, 2014, Enhanced imaging with high-resolution full-waveform inversion and reverse time migration: A North Sea OBC case study: The Leading Edge, **33**, no. 9, 986–992, http://dx.doi.org/10.1190/tle33090986.1.

Ray, S., Z. Zhang, Z. Fu, L. Liu, and P. Wang, 2014, Noise attenuation using a dipole sparse Tau-P inversion: 84th Annual International Meeting, SEG, Expanded Abstracts, 4213–4217, http://dx.doi.org/10.1190/segam2014-1194.1.

Tarantola, A., 1984, Inversion of seismic reflection data in the acoustic approximation: Geophysics, **49**, no. 8, 1259–1266, http://dx.doi.org/10.1190/1.1441754.

Thomsen, L. A., 1986, Weak elastic anisotropy: Geophysics, **51**, no. 10, 1954–1966, http://dx.doi.org/10.1190/1.1442051.

Virieux, J., and S. Operto, 2009, An overview of full-waveform inversion in exploration geophysics: Geophysics, **74**, no. 6, WCC1–WCC26, http://dx.doi.org/10.1190/1.3238367.

Warner, M., A. Ratcliffe, T. Nangoo, J. Morgan, A. Umpleby, N. Shah, V. Vinje, I. Stekl, L. Guasch, C. Win, G. Conroy, and A. Bertrand, 2013, Anisotropic 3D full-waveform inversion: Geophysics, **78**, no. 2, R59–R80, http://dx.doi.org/10.1190/geo2012-0338.1.

Warner, M., and L. Guasch, 2014, Adaptive waveform inversion — FWI without cycle skipping — Theory: 76th Conference and Exhibition, EAGE, Extended Abstracts, We E106 13, http://dx.doi.org/10.3997/2214-4609.20141092.